33rd Annual International Conference of the IEEE EMBS
Boston, Massachusetts USA, August 30 - September 3, 2011

Maximal Curvature-based Segmentation of 3D Vessel Contours

K. Krissian F. Santana-Jorge J. Esclarín-Monreal M. Maynar-Moliner J.M. Carreira-Villamor

Abstract— **The segmentation of three-dimensional vascular trees is an important topic in medical image processing. Although it may seem to be an easy task, many different techniques have been proposed in the literature during the last decade and many difficulties remain. One can wonder why the human eye is usually able to understand the connectivity and the topology of the different structures while most algorithms fail to do so. In this paper, we propose an original approach that classifies the different contours by applying a geodesic distance transform on the contours of the vessels, where the evolution speed depends directly on the maximal curvature of the contours. This proposition comes from the observation that the maximal curvature on a standard vessel is usually positive and almost constant while it approaches zero or becomes negative on the contour at the contact with other structures. We describe our method in details and present promising results on synthetic and real images, where the method has been able to detect complex vascular structures without leaking into bones or mixing different vascular networks.**

I. INTRODUCTION

The segmentation of vascular structures is a fundamental step for many applications in medical image processing, among them are endovascular surgery planning and simulation, diagnosis of vascular diseases like aneurysms and stenosis. It can also help in surgery like liver resection, or in the brain to avoid damaging important vessels. In some cases where the contrast of the vascular structures is good and they are isolated from other structures of similar intensities, their segmentation can be relatively easy and many algorithms can obtain satisfactory results. However, in general, this process is more difficult than it seemed to be. Figure 1 depicts complex arteries and veins trees, using Volume Rendering from a Computed Tomography Angiography (CTA) of the neck. One of the difficulties in the segmentation process is to separate the different vascular structures and to avoid leaks into non vascular structures like bones.

A. Previous work

Reviews on vascular structures segmentation are presented in [1], [2], [3]. Among the different techniques are methods for enhancing and detecting the vessels centerlines, based on linear multiscale analysis [4], [5] and on minimal cost path [6], methods based on the level-set active contour evolution [7], [8], [9], methods based on statistical framework, on graph cuts algorithms [10], particle filters and template matching [11]. The diversity of the proposed methods and the number of publications demonstrate the level of difficulty to obtain a robust and reliable technique with minimal or no user-interaction. Despite the quality of the different reviews to describe the current literature on this topic, the comparison of several methods is a difficult task and several challenges have been organized to compare 3D vascular segmentation techniques on CTA of Coronary arteries [12], and Carotid bifurcation [13]. While these two challenges proposed to compare methods from several categories: manual, semi-automatic and fully automatic methods, most of the proposed methods fall within the semi-automatic category where the experts have selected a seed point within the main vascular trunk and other points within each branch of the desired three-dimensional vascular tree. Despite the initial points selected by the physicians, the task of extracting the path of the vascular tree prove to be difficult in many cases due to the complexity of the vascular networks, to interwoven vascular trees, to calcifications and stenosis and vascular anomalies, variations between patients and tortuosities. However, when interactively looking at a volume dataset using a volume or surface rendering with adequate parameters, the human observer is usually able to follow the correct path of the vascular structures. This can be explain by the a priori understanding of the tree structure, including the notion of branching, stenosis, calcification and continuity within the 3D vessels contours which allow the observer to understand the three-dimensional scene. In this work, we introduce an new algorithm that helps understanding the three-dimensional structures of the vessels by taking into account the continuity of their contours. One of the main aim of this algorithm is to be able to separate and partition several interwoven vascular tree, enabling a better understanding of the patient scan that could be used for visualization, quantification or any posterior image processing task.

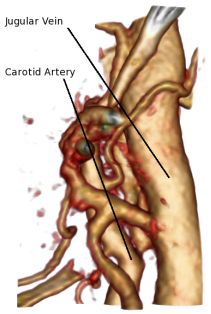

Fig. 1. Interwoven vascular trees.

II. METHODOLOGY

The proposed method is based on the observation that the distribution of the maximal curvature along the contours of the vessels gives a strong hint on the presence of

This work has been supported by the project SIMVA, TIN2009-10770 from the Spanish Ministry of Science and Innovation, and from the program Ramón y Cajal.

K. Krissian, F. Santana-Jorge, J. Esclarín-Monreal and M. Maynar-Moliner are with Universidad de Las Palmas de Gran Canaria, Spain. {krissian,jesclarin}@dis.ulpgc.es, francisco.jesus.santana@gmail.com, mmaynar@hotmail.com

J.M. Carreira is with the Universidad de Santiago de Compostela, Spain. josemartin.carreira@usc.es

close or touching structures that don't belong to the current tracked vessel. Based on this observation, we design an algorithm that first computes the voxels belonging to the vessels contours, then, starting from several manual initial points within the contours of distinct tubular trees, we evolve competing fronts within the contours and using a maximal curvature based propagation speed, until reaching a given maximal evolution time. As a result of this process, we obtain several connected sets of contour voxels where each set should belong to a different vascular structure if the speed function has accomplished its function, which is to prevent evolution of the front at the contact between the different structures. These different sets of voxels are then processed to create several three-dimensional representations of each of the recognized vascular structures, depicting a partitioning of the contours.

A. *Distribution of the principal curvatures on the contours*

The principal curvatures at any voxel with non-zero gradient of the image are defined as the principal curvatures of the iso-surface passing through this voxel. If one defines a unit vector in the plane orthogonal to the gradient at the current voxel, this vector and the gradient vector form a plane that cuts the isosurface into a curve with a given curvature at the current voxel. The orientations that give the maximal and the minimal values of this curvatures are orthogonal, and are named the maximal and the minimal directions of curvatures respectively and their corresponding curvatures are the maximal and the minimal curvatures at this voxel. We define the interior of the object as the bright side of the isosurface, and convex object are defined with positive curvatures while concave object will have negative curvatures. The principal curvatures (resp. the principal directions of curvature) can be obtained as two of the eigenvalues (resp. eigenvectors) of the following matrix:

$$H' = \frac{-1}{\|\nabla_\sigma u\|} P H_\sigma P \text{ with } P = I - \eta^* \eta^{*t},$$

where H_σ is the Hessian matrix of the smoothed image obtained by convolution of the image with derivatives of the Gaussian kernel of standard deviation σ, I is the identity matrix in 3D, and η^* is a unit vector in the gradient direction $\eta^* = \frac{\nabla_\sigma u}{\|\nabla_\sigma u\|}$ (also obtained from Gaussian convolution). One of the eigenvectors of this matrix is the gradient of the smoothed image with a zero associated eigenvalue, and the two others are the principal curvature directions. We will be denote κ_{min} and κ_{max} the two principal curvatures so that κ_{min} is lower than κ_{max} in absolute value, i.e. $|\kappa_{min}| \leq |\kappa_{max}|$. It is interesting to look more closely at the distribution of the principal curvatures on the surface of tubular objects and tubular trees. Figure 2 depicts the principal curvatures of several synthetic tubular structures, computed on three-dimensional synthetic datasets and displayed in colors on the contours of the studied objects. A rainbow colormap has been selected to represent the values of the principal curvatures within a range of [-0.5,0.85] which is a relevant range of values for our applications. As expected, in

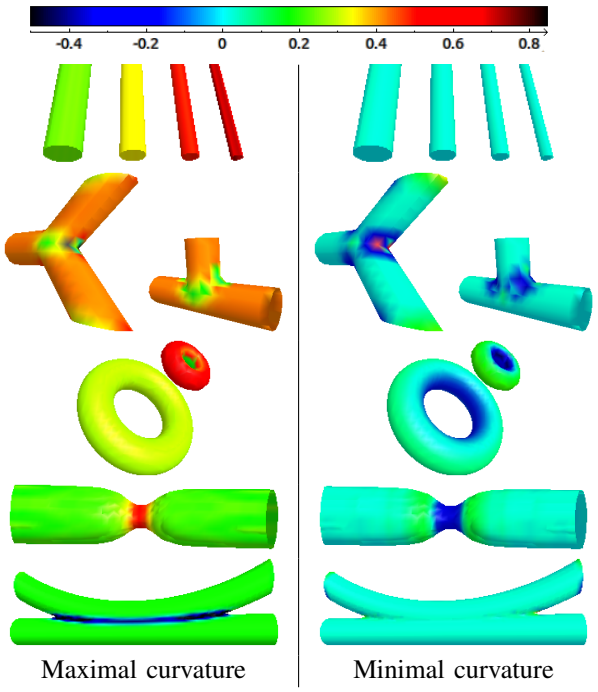

Fig. 2. Look-up Table and principal curvatures on synthetic tubular images.

the case of a circular straight cylinder, the maximal curvature reflects the inverse of the cylinder radius and the minimal curvature is zero at every location of the contours. Note that the principal curvatures are well defined at the object contour, where the image gradient is high, and are ill-defined at the center of the vessels where the gradient passes through zero. In the cases of torus with different curvatures, the maximal curvature still represents the inverse of the cylinder radius, while the minimal curvature on the contour is ranges from negative (inner part) to positive values (outer part) depending on the location on the contour. Vascular junctions create discontinuities with lower values of both curvatures on part of the junction, at some location of the surface junction, the maximal curvature can even become negative. In the case of our synthetic stenosis, the maximal curvature increases due to the lower radius of the tube at the stenosis, while the minimal curvature becomes negative due the concavity. The lower row of fig. 2 depicts the case of tangent tubular structures. In this case and in general for tangent structures involving tubular shape, the area of contact on the contours between the two different structures depicts negative values of the maximal curvature while the minimal curvature can have positive or negative values in this area. As a conclusion and based on these observations, we use only the maximal curvature to track the topology of the vascular networks on their contours and we will assume that the contact between a three dimensional vascular networks and another structure will create a closed curve of negative values of the maximal curvature, allowing to separate the different structures, while there will usually exists a path of non-negative maximal curvatures values between any two locations of positive maximal curvatures on the same vascular tree. Although this assumption may not be fulfilled in all cases, we will use it as a base to develop an algorithm that is able to split a

vascular tree from other structures and facilitate the posterior segmentation and understanding of the volumetric data. In fig. 3, we display the results of computing the maximal curvature, using the same colormap as in fig. 2, on two different real CTA volumes of the abdomen (left) and of the Carotid arteries (right). Since the aorta on the left image is a vessel with a big diameter, the curvature was calculated using a Gaussian standard deviation of 2 to reduce the noise and the possible negative maximal curvatures that it can create on the vessel surface. In both images, we can notice that our hypothesis on the distribution of the maximal curvature is fulfilled. On the carotid image at the right, the negative values of the maximal curvature at the contact between different vascular structures or between vascular structures and bones are clearly rendered.

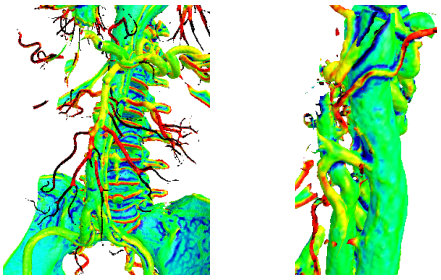

Fig. 3. Maximal curvatures on real data sets of the Aorta and the Carotid.

B. Design of the propagation speed

We choose to apply the following function to the maximal curvature value κ_{max}:

$$W_\kappa(\kappa_{max}) = \begin{cases} 0 & \text{if} \quad \kappa_{max} < l_1, \\ l_2 & \text{if} \quad l_1 <= \kappa_{max} < l_2, \\ \kappa_{max} & \text{if} \quad l_2 <= \kappa_{max} < h, \\ h & \text{if} \quad \kappa_{max} >= h, \end{cases} \tag{1}$$

where l_1, l_2 and h are set respectively to -0.2, 0.01, and 1. Which means that we completely prevent the front from evolving at values lower than -0.2, we allow very slow evolution between -0.2 and 0.01, we allow an evolution proportional to the maximal curvature for values between 0.01 and 1 and we clamp the maximal speed to 1 for maximal curvatures higher than 1. This choice of evolution speed allows to demonstrate the utility of the proposed method, even though other functions could be used in this case.

C. Implementation details

The propagation of the different fronts has been implemented using the Fast Marching [8] method directly on the three-dimensional volume. Another option is to evolve on a precomputed mesh that would include the contours of interest. For the purpose of our method, we need a selection of the voxels located at the image contours, and if possible, mainly at the contours of vascular structures. We use the local maxima of local image intensity variance as a characteristic of the contours, since it can directly be related to the properties of the noise in the image while the variability of image gradient magnitude is more difficult to apprehend. The calculation of the local variance of the image intensity is weighted by a Gaussian kernel, and then its expression can be computed as:

$$V_\sigma(I) = G_\sigma * I^2 - (G_\sigma * I)^2. \tag{2}$$

This expression, as compared to using a box-like neighborhood, introduces a continuous scale parameter σ, which is set to 0.7 voxel in our experiments.

A simple procedure based on linear interpolation is used to extract the local maxima of V_σ in the direction of the image gradient, this procedure consists in computing the image gradient $\nabla_\sigma I$ from convolution with Gaussian derivatives, and in selecting the voxels whose intensity is higher that their two neighbors in the direction of the gradient and at a distance of half a voxel:

$$V_{max}(\mathbf{x}) = \begin{array}{l} V_\sigma(\mathbf{x}) \text{ if } \begin{cases} V_\sigma(\mathbf{x}) > V_\sigma(\mathbf{x} + \frac{\xi}{2}) \text{ and} \\ V_\sigma(\mathbf{x}) > V_\sigma(\mathbf{x} - \frac{\xi}{2}) \end{cases} \\ 0 \text{ otherwise,} \end{array} \tag{3}$$

where $\xi = \frac{\nabla_\sigma I}{\|\nabla_\sigma I\|}$. The advantage of limiting the evolution of the voxels of the contour is to limit the risk of leakage of the front, however, the Fast Marching algorithm is not especially designed to evolve on a thin surface but on a volume, so we add one layer of voxels around the selected contour voxels on the side of the gradient (since vessels are usually brighter that their background). The resulting image, where the selected voxels at or close to the contours have a value of 1 and the other voxels a value of 0, is denoted M.

$$M(\mathbf{x}) = \begin{cases} 1 \text{ if } V_{max}(\mathbf{x}) > \mathbf{0} \text{ or} (\mathbf{V_{max}}(\mathbf{x} - \xi/\mathbf{2}) > \mathbf{0} \\ \quad \text{and} \quad I(\mathbf{x} + \xi/\mathbf{2}) \in [\mathbf{I_{min}}, \mathbf{I_{max}}]), \\ 0 \text{ otherwise;} \end{cases} \tag{4}$$

where $[I_{min}, I_{max}]$ is the a user-defined intensity range of the vessel intensities, this way we can pre-select contours that contains on their higher intensity side a possible vascular intensity value.

An interesting feature used to remove noise or to detect edges is the coefficient of variation, based on the local statistics of the image [14]. In our case of CTA data, we will make the hypothesis that the noise is uncorrelated, additive and Gaussian of zero mean and standard deviation σ_n, which can be estimated from a region of the same tissues within the image. In this case, we can estimate the local variation of the image intensity without noise as $var(f) = var(g) - \sigma_n^2$, where $g = f + n$ is the observed signal and f is the theoretical signal without noise. We define a term for the propagation speed based on the local statistics as the ratio between the local variance of the image without noise and the local variance of the observed image, this propagation term, denoted S_c, is written as:

$$S_c = \max(0, V_\sigma - \sigma_n^2)/V_\sigma. \tag{5}$$

Our final evolution speed image, denoted F, is defined as the product of the three images previously defined:

$$F = W_\kappa(\kappa_{max}) \times S_c \times M. \tag{6}$$

Starting from n user defined initial seed points, the eikonal equation $\|\nabla T\| = F$ is solved up to a maximal time T_{max}

and keeping track of the closest initial point in the geodesic distance sense for each computed voxel value of the evolution time image T. The result is a partition of the contours in n components that should ideally contain only contours of same vascular trees. Polygonal meshes representing the local maxima of V_σ are extracted from the zero-crossings of the scalar product $\nabla V_\sigma . \nabla_\sigma I$ within each classified contour component and they are rendered in 3D with different colors.

III. RESULTS

Figure 4 shows the result of applying the proposed technique a neck CTA. The user initially selected three points on contour of the Common Carotid Artery (in red), of the Internal Carotid Artery (in orange), and of the Jugular Vein (in blue). Each of the point has evolved with the contour voxels and the algorithm has been able to separate correctly the jugular vein from the different arteries at the several locations of contact. It has also been able to avoid entering bones that come into contact with the jugular vein at the top of the image. Due to a strong stenosis, the branching of the common carotid artery into the external and the internal carotid artery has not been fully reconstructed, but the algorithm has fulfilled its purpose, which is to separate different vascular networks. Figure 5 depicts the result of the algorithm on a selected sub-volume of $293 \times 255 \times 944$ voxels from an abdominal CTA, where three initial seed points have been selected, two of them in the aorta and one in the heart. The algorithm has been able to grow within the vascular network without leaking into the bones from the hip or the vertebral column, permitting a good visualization of the vascular tree. Moreover, the contours of the heart and of the pulmonary vessels have been detected separately, allowing a visualization of the dissected aorta alone.[1]

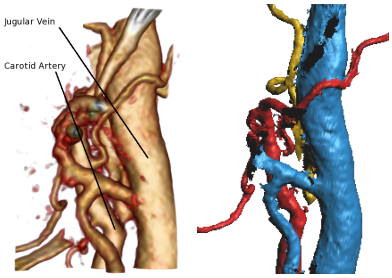

Fig. 4. Contour segmentation from neck CTA starting from 3 points.

IV. CONCLUSIONS AND FUTURE WORKS

We have proposed and described a novel approach to partition the contours of vascular structures from three-dimensional data sets, with the aim of separating interwoven tubular networks and to avoid leakage from a vessel to other touching structures. Our technique relies strongly on the properties of the maximal curvature along the contours of tubular structures and especially on the fact that it becomes negative at the contact with other structures while there exists a path of non-negative maximal curvature values within different location of the contours of the same vascular network. Our first results on neck and abdominal datasets, displaying highly interconnected and complex networks are very encouraging. Future works include an automatic selection of the seed points and a full segmentation of the detected vessels including the lumen inside the detected contours.

[1]All the figures have been generated using AMILab (http://amilab.org).

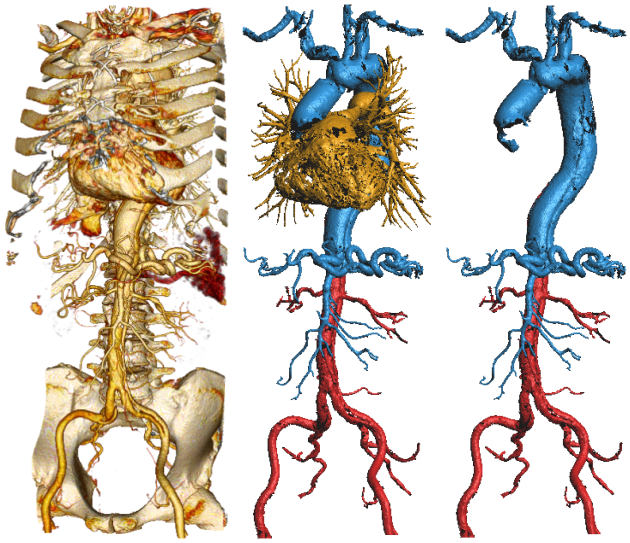

Fig. 5. Contour segmentation on thoraco-abdominal and pelvic CTA starting from 3 points. The heart and the pulmonary vessels are separated from the aorta in a patient dissection in the thoraco-abdominal aorta.

REFERENCES

[1] C. Kirbas and F. Quek, "A review of vessel extraction techniques and algorithms," *ACM Computing Surveys*, vol. 36, pp. 81–121, 2004.

[2] J. Suri, *et al.*, "Shape recovery algorithms using level sets in 2-d/3-d medical imagery: a state-of-the-art review," *IEEE Trans. on Information Tech. in Biomedicine*, vol. 6, no. 1, pp. 8–28, Mar 2002.

[3] D. Lesage, *et al.*, "A review of 3d vessel lumen segmentation techniques: Models, features and extraction schemes," *Med. Image Anal.*, vol. 13, no. 6, pp. 819–845, 2009.

[4] K. Krissian, *et al.*, "Model based detection of tubular structures in 3d images," *Computer Vision and Image Unders.*, vol. 80, no. 2, pp. 130–171, nov 2000.

[5] A. Frangi, *et al.*, "Multiscale vessel enhancement filtering," in *MICCAI'98*, ser. Lecture Notes in Computer Science, W. Wells, A. Colchester, and S. Delp, Eds., vol. 1496, oct 1998, pp. 130–137.

[6] T. Deschamps and L. Cohen, "Fast extraction of minimal paths in 3d images and application to virtual endoscopy," *Med. Image Anal.*, vol. 5, no. 4, Dec. 2001.

[7] L. M. Lorigo, *et al.*, "Curves: Curve evolution for vessel segmentation," *Med. Image Anal.*, vol. 5, pp. 195–206, 2001.

[8] J. Sethian, *Level Set Methods and Fast Marching Methods: Evolving Interfaces in Computational Geometry, Fluid Mechanics, Computer Vision and Materials Science*. Cambridge University Press, 1999.

[9] X. Wu, *et al.*, "Segmentation and reconstruction of vascular structures for 3d real-time simulation," *Med. Image Anal.*, vol. 15, no. 1, pp. 22–34, 2011.

[10] M. Schaap, *et al.*, "Coronary lumen segmentation using graph cuts and robust kernel regression," in *Information Processing in Medical Imaging*, ser. Lecture Notes in Computer Science. Springer Berlin / Heidelberg, 2009, vol. 5636, pp. 528–539.

[11] O. Friman, *et al.*, "Multiple hypothesis template tracking of small 3d vessel structures," *Med. Image Anal.*, vol. 14, no. 2, pp. 160–171, 2010.

[12] M. Schaap, *et al.*, "Standardized evaluation methodology and reference database for evaluating coronary artery centerline extraction algorithms," *Med. Image Anal.*, vol. 13, no. 5, pp. 701–714, 2009.

[13] K. Hameeteman, *et al.*, "Evaluation framework for carotid bifurcation lumen segmentation and stenosis grading," *Med. Image Anal.*, vol. In Press, Corrected Proof, pp. –, 2011.

[14] Y. Yu and S. T. Acton, "Edge detection in ultrasound imagery using the instantaneous coefficient of variation," *IEEE Trans. Med. Imag*, vol. 13, pp. 1640–1655, 2004.